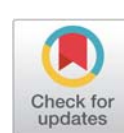


REPORT DOCUMENTATION PAGE

Form Approved
OMB No. 0704-0188

Public reporting burden for this collection of information is estimated to average 1 hour per response, including the time for reviewing instructions, searching existing data sources, gathering and maintaining the data needed, and completing and reviewing this collection of information. Send comments regarding this burden estimate or any other aspect of this collection of information, including suggestions for reducing this burden to Department of Defense, Washington Headquarters Services, Directorate for Information Operations and Reports (0704-0188), 1215 Jefferson Davis Highway, Suite 1204, Arlington, VA 22202-4302. Respondents should be aware that notwithstanding any other provision of law, no person shall be subject to any penalty for failing to comply with a collection of information if it does not display a currently valid OMB control number. **PLEASE DO NOT RETURN YOUR FORM TO THE ABOVE ADDRESS.**

| | | | | | |
|--|------------------------------------|---|-----------------------------------|---|---|
| 1. REPORT DATE (DD-MM-YYYY) DD-MM-YYYY | | 2. REPORT TYPE Conference Paper | | 3. DATES COVERED (From - To) | |
| 4. TITLE AND SUBTITLE The Response of Cryogenic H ₂ /O ₂ Coaxial Jet Flames to Acoustic Disturbances (POST PRINT) | | | | 5a. CONTRACT NUMBER | |
| | | | | 5b. GRANT NUMBER | |
| | | | | 5c. PROGRAM ELEMENT NUMBER | |
| 6. AUTHOR(S) David J. Forliti (Sierra Lobo); A. Badakhshan (ERC); Jeffrey L. Wegener (Physical Sciences, Inc.); Ivett A Leyva (AFOSR/RTE); Douglas G. Talley | | | | 5d. PROJECT NUMBER | |
| | | | | 5e. TASK NUMBER | |
| | | | | 5f. WORK UNIT NUMBER Q0YA | |
| 7. PERFORMING ORGANIZATION NAME(S) AND ADDRESS(ES) Air Force Research Laboratory (AFMC) AFRL/RQRC 10 E. Saturn Blvd Edwards AFB, CA 93524 | | | | 8. PERFORMING ORGANIZATION REPORT NO. | |
| 9. SPONSORING / MONITORING AGENCY NAME(S) AND ADDRESS(ES) Air Force Research Laboratory (AFMC) AFRL/RQR 5 Pollux Drive Edwards AFB, CA 93524 | | | | 10. SPONSOR/MONITOR'S ACRONYM(S) | |
| | | | | 11. SPONSOR/MONITOR'S REPORT NUMBER(S) AFRL-RQ-ED-TP-2014-348 | |
| 12. DISTRIBUTION / AVAILABILITY STATEMENT Approved for public release; distribution unlimited | | | | | |
| 13. SUPPLEMENTARY NOTES AIAASciTech Forum; 5-9 January 2015; Kissimmee, FL; 53 rd AIAA Aerospace Meeting. PA Case Number: 14595; Clearance Date: Dec 12, 2014. AIAA 2015-1607; DOI: 10.2514/6.2015-1607 The U.S. Government is joint author of the work and has the right to use, modify, reproduce, release, perform, display, or disclose the work. | | | | | |
| 14. ABSTRACT An experimental study has been conducted to explore the coupling between a coaxial gaseous hydrogen / liquid oxygen jet flame and transverse acoustic perturbations. A variety of chamber conditions including acoustic frequency, amplitude, and the location of the pressure node / antinode with respect to the flame were examined. The flame response was documented using high-speed imaging including backlit visualization and unfiltered chemiluminescence. Dynamic mode decomposition was used to isolate the spatial structure of the flame response at the forcing frequency. The results indicate that the flame response to forcing is qualitatively similar to previous results of nonreacting coaxial jet flows; the pressure node forcing appears to generate in-plane flapping of the flame while pressure antinode forcing induces a helical structure in the flame. | | | | | |
| 15. SUBJECT TERMS | | | | | |
| 16. SECURITY CLASSIFICATION OF: | | | 17. LIMITATION OF ABSTRACT | 18. NUMBER OF PAGES | 19a. NAME OF RESPONSIBLE PERSON |
| a. REPORT Unclassified | b. ABSTRACT Unclassified | c. THIS PAGE Unclassified | | | 19b. TELEPHONE NO (include area code) |



The Response of Cryogenic H₂/O₂ Coaxial Jet Flames to Acoustic Disturbances

David J. Forliti¹

Sierra Lobo, Inc. Edwards AFB, CA 93524

A. Badakhshan²

ERC Inc. Edwards AFB, CA 93524

Jeffrey L. Wegener³

Physical Sciences Inc., Andover, MA 01810

Ivett A. Leyva⁴

AFOSR/RTE Arlington, VA 22203

and

Douglas G. Talley⁵

AFRL/RQRC, Edwards AFB, CA 93524

An experimental study has been conducted to explore the coupling between a coaxial gaseous hydrogen / liquid oxygen jet flame and transverse acoustic perturbations. A variety of chamber conditions including acoustic frequency, amplitude, and the location of the pressure node / antinode with respect to the flame were examined. The flame response was documented using high-speed imaging including backlit visualization and unfiltered chemiluminescence. Dynamic mode decomposition was used to isolate the spatial structure of the flame response at the forcing frequency. The results indicate that the flame response to forcing is qualitatively similar to previous results of nonreacting coaxial jet flows; the pressure node forcing appears to generate in-plane flapping of the flame while pressure antinode forcing induces a helical structure in the flame.

I. Introduction

COMBUSTION instability is one of the critical phenomena that impacts the design, performance, and robustness of energy and propulsion systems. Due to the extreme conditions, liquid rocket engines (LREs) suffer from potentially extreme consequences under unstable conditions, including rapid wear of components and catastrophic failure. Combustion instability is governed by a coupling between propellant injection and mixing, subsequent chemical reaction, and pressure fluctuations. There are multiple coupling mechanisms that are possible, which leads to a variety of combustion instability classifications.¹ Accounting for all combustion instability mechanisms during the engine development process is currently not possible, due in part to a lack of knowledge of the fundamental interactions between fluid dynamics, combustion, and pressure fluctuations. The purpose of the current research is to contribute to this understanding for injector types and operating conditions relevant to LREs. The research, which is

¹ Research Scientist, Sierra Lobo, Inc., 10 E. Saturn Blvd, Building 8451, Edwards AFB, CA 93524, senior member.

² Research Scientist, RQRC, Combustion Devices Group, 10 Saturn Blvd., Edwards AFB, CA 93524.

³ Former Graduate Student, Department of Mechanical and Aerospace Engineering, UCLA, Los Angeles, CA 90095 student member.

⁴ Aerothermodynamics PO, AFOSR/RTE, 875 N Randolph St, Arlington, VA 22203, Associate Fellow.

⁵ Lead, Combustion Dynamics Group, AFRL/RQRC., 10 E. Saturn Blvd, Building 8451, Edwards AFB, CA 93524, Associate Fellow.

Approved for public release; distribution unlimited.

experimental in nature, will also generate a database that is needed to validate both low- and high-fidelity rocket engine design tools.

Previous work at AFRL has made major contributions towards understanding the coupling between acoustic waves and rocket injector flows in a *nonreacting* regime.²⁻⁹ These experiments employed a high-pressure test facility that allowed for investigation of coaxial jets flowing inert surrogates, generally gaseous, liquid, and supercritical nitrogen, and exposing this shear flow to a variety of acoustic conditions that are representative of a transverse resonance that would occur in a rocket engine. In subcritical conditions, the center flow of the coaxial jet is cooled to a liquid condition, while the outer annular flow is chilled but maintained as a gas. This configuration is relevant to coaxial jet injectors for O_2/H_2 LREs such as the Space Shuttle Main Engine (SSME). The fluid surrogates were selected and conditioned to have relevance to LRE conditions in terms of the momentum flux ratio, density ratio, velocity ratio, and thermodynamic state (subcritical or supercritical). The geometry of the coaxial injectors was also varied. At sufficiently-elevated pressure, the fluids may experience supercritical behavior where no phase transition between the liquid-like and gas-like regions exist. The subcritical and supercritical behavior is easily characterized for single component mixtures because the critical point is fixed. When a multi-component system is considered, the description of the flow regime is more complicated because the critical point now depends on the composition of the mixture which varies in space and time.³ The results of this large body of work highlights the manner in which the mixing can be modulated through a one-way coupling between the acoustic field and the fluid mechanics. This provides some insight on the combustion instability mechanism as this interaction plays an important role in the feedback mechanism. What is unclear is how the presence of heat release contributes to the interaction between the fluid mechanics and the acoustics. Additionally, the resultant combustion dynamics which are driven by the fluid mechanics and the acoustics plays a role as unsteady heat release can feed back and amplify the acoustic field. Thus the natural evolution of this research campaign is to introduce heat release into the physics.

The present research employs a new experimental facility at AFRL that is capable of investigating the coupling between acoustic waves and rocket injector flames. The results are preliminary and exploratory, and consider the response of a flame to a variety of acoustic environments, including acoustic frequency and location within the mode shape. The qualitative features of the flames both with and without acoustics are presented, and dynamic mode decomposition (DMD) was applied to isolate the response of the flame at the forcing frequency.

II. Background

The last decade has seen a variety of efforts exploring rocket injector flame dynamics in the presence of tuned or induced acoustic resonance. Anderson and coworkers have been investigating longitudinal combustion instabilities in the Continuously Variable Resonance Chamber (CRVC), with parallel computational efforts.¹⁰⁻¹² Anderson's group has also been exploring transverse instabilities using a linear array of injectors with the outer-most injectors designed to be unstable to drive a transverse mode in the combustion chamber.¹³⁻¹⁵ These efforts have focused on swirl-coaxial injectors operating with various oxidizer/hydrocarbon combinations. High-amplitude pressure fluctuations were observed for these experiments.

Experiments in Europe have also focused on exploring the flame response of rocket chambers experiencing different types of induced acoustic modes.¹⁶⁻²² These studies employed a common methodology for establishing acoustic resonance that involved periodic blocking of a secondary exhaust nozzle. The periodic flow through the secondary nozzle results in chamber pressure fluctuations that when properly tuned can drive an acoustic resonance in the chamber. Dramatic large-scale flame motions have been observed in most of these studies.

The current work complements these efforts in exploring the coupling mechanisms between rocket injector flames and an acoustic resonance. The current effort considers a single shear coaxial injector with cryogenic oxygen in the inner flow and cooled gaseous hydrogen in the outer annular flow. This conserves tracability to the large body of work done over the past decade at AFRL under nonreacting conditions, which will allow insight on the role of heat release in the flow response. This tracability also helps frame the manner in which nonreacting data scales to reacting flow conditions. Unlike many of the efforts cited above, focus is not placed on highly forced conditions (where pressure fluctuations scale with the mean chamber pressure), but instead on identifying the conditions where the coupling is first detectable as well as exploring the coupling sensitivity to forcing parameters.

III. Experimental Details

A schematic and design rendering of the facility is shown in Fig. 1. A single injector element is considered in the present study, and is located in the middle of a rectangular test section. A gaseous nitrogen coflow and window cooling flow are used to condition the test area and protect the chamber windows, respectively. Two piezoelectric sirens from Piezo Systems, Inc. are located laterally with respect to the combustion zone and are used to establish

transverse acoustic standing waves. These sirens are excited through the use of an amplified signal generator. The exhaust of the inner chamber mixes with gaseous nitrogen flow in the outer chamber, and the combined flow passes through an exhaust orifice that controls the chamber pressure. The propellants are supplied from compressed gas tanks at ambient temperature. An oxygen heat exchanger, designed and fabricated by Sierra Lobo, Inc., along with a hydrogen heat exchanger designed in-house are used to cryogenically condition each propellant flow. Ignition is achieved via a novel ignition system that will be described in future publications due to patent-related issues. Further background on the facility is described by Wegener et al.⁷

A variety of coaxial jet injector models have been investigated at AFRL under nonreacting flow conditions.^{9, 23} The coaxial jet injector geometry and near field flow dynamics are illustrated in Fig. 2. For H_2/O_2 reactants at typical injection velocities, the flame is expected to be stabilized downstream of the blunt trailing edge between the inner and outer flows (referred to as the LOx post tip or just post tip).²⁴⁻²⁸ The various length scales of the subject injector indicated in Fig. 2 are tabulated in Table 1. These dimensions can be converted into two dimensionless groups, the outer-to-inner area ratio AR of 1.68, and the dimensionless post thickness t/D_1 of 0.27. The injector flow passages are sufficiently long to ensure fully-developed turbulent flow at the injector exit.

High framerate images were captured using a Phantom 7.10 camera at a frame rate of 20 kHz. Backlit flow visualization and unfiltered chemiluminescence were employed to characterize the natural and forced reacting flow response. Filtered chemiluminescence will be employed in future studies to isolate OH* emission. A statistical analysis of the images allows for exploration of the spatial and temporal structure of the reacting flow field. Dynamic mode decomposition³¹ was employed to extract the flame response to the acoustic forcing. The relative amplitude of the forced mode to the remaining modes of the decomposition are used as a qualitative indicator of relative strength of the forcing response.

A single set of nominal injector operating conditions was considered for the present study. Table 2 summarizes the nominal operating conditions, including propellant temperatures, momentum flux ratio, oxygen to fuel mixture ratio MR, and Reynolds numbers. The chamber pressure was 3.4 kPa (500 psi) which is thermodynamically subcritical for oxygen; thus two-phase flow behavior is expected. The acoustic forcing is characterized by the frequency in kHz, the location of the injector, being either at a pressure node or a pressure antinode, and the driving voltage amplitude (prior to amplification). Acoustic pressure measurement was not possible during the current set of tests, but will be done in future studies.

IV. Results

One of the primary objectives of the current project is to understand the impact the flame imposes on the flow field. Figure 3 shows a series of images of both the nonreacting and reacting flows without acoustic forcing. The images shown in Fig. 3a are backlit images showing the liquid oxygen core and the annular hydrogen flow. In these studies, the backlighting was reduced to avoid contamination of the chemiluminescence for reacting cases. The nonreacting case represents a situation where the flow was not ignited. The dark region in the bottom half of the image is due to nonuniformities in the backlighting. The qualitative features of the inner jet topology are generally representative of past nonreacting flow studies. This particular sequence shows the breaking and downstream convection of a liquid oxygen section at the end of the dark core. This breaking off of a liquid segment appears to occur in an aperiodic manner. The unfiltered chemiluminescence images shown in Fig. 3b that the emission from the first few diameters is relatively weak compared to the downstream region. This is in part due to fogging of the test chamber window, fogging which does not exist in the downstream region potentially due to heat from the flame. The sequence of images suggests that unsteady burning is present, as would be expected due to the turbulent operating conditions associated with fully-developed flow, and the evolution of the flame topology is resolved. Burning structures appear to move slowly downstream with increasing time. The presence of liquid oxygen within the flame is unclear for the unforced case. Future high-intensity spark backlit shadowgraph imaging will be used to identify the topology of the liquid oxygen inner core.

Over 2000 images were collected for each test case at a frame rate of 20 kHz. Thus the sequence of images can be analyzed to extract spatial and temporal content. For the nonreacting case, spectral analysis was done on the temporal signals from the pixels located near the interface between the liquid oxygen and gaseous hydrogen. This measures the frequencies present in the inner shear layer region. Figure 4 shows the local spectra for the nonreacting case shown in Fig. 3a. The figure shows the axial evolution of the spectra of the images as a function of downstream distance. Although noisy, some spectral peaks are evident; the noise is due to the fact that the temporal data is limited to only 2000 samples. The peak indicated by the vertical blue line at x/D_1 of four and seven is likely to be the signature of structures in the inner shear layer. This peak persists to x/D_1 of seven, but disappears at eight, which is downstream of the dark core. Although the contrast is weaker in the downstream region, the image fluctua-

tions still represent the presence of structures that contain density differences. The preferred mode of the coaxial jet, based on the scaling law of Wegener²⁹, is shown on the figure as the red vertical line and is near 1 kHz. The preferred mode estimate of 1 kHz is generally representative of lower frequency peaks at x/D_1 of seven and eight.

Figure 5 shows the spectral content of the chemiluminescence signals for the flame shown in Fig. 3b at the same axial locations shown in Fig. 4 for the nonreacting case. The power spectral density (PSD) plots show both the reacting (blue line) and nonreacting (gray) cases. The spectral peak of 2.5 kHz observed at $x/D_1 = 4$ for the nonreacting case is no longer evident, while a moderate peak has emerged at approximately 3.5 kHz; the new apparent shear layer frequency is indicated by the blue vertical line. This indicates a possible frequency shift of the shear layer mode, indicated by the arrow on the figure, from lower to higher frequency due to the presence of the flame. Although there is no obvious flame signature present in the images at this axial location, there is a low-level light signal detected. This potential frequency shift will be explored further in future work.

The PSDs at the x/D_1 of seven and eight show some strong peaks that are below 2 kHz. For the reacting cases, there are multiple peaks at about 850 Hz and 1300 Hz, as well as a lower frequency that emerges at the downstream location. These peaks are in the same general range as the nonreacting preferred mode of 1 kHz. There is a peak at approximately 400 Hz, that emerges at $x/D_1 = 8$. This new peak may be a discrete phenomenon or may be the result of nonlinear interaction between the two higher frequencies. The evolution of the spectra further downstream is shown in Fig. 6. The spectra span a range of x/D_1 from nine to thirteen. The spectral trend shows a general shift to lower frequencies with increasing downstream distance, which is expected due to growth of the reacting structure length scales. A consistent peak around 500 Hz and indicated by the red vertical line is seen in the downstream region. The tilted green line shows the broadband energy-containing spectral range is shifting to lower frequency with increasing downstream distance.

Overall, the spectral analysis suggests that the frequency content in the coaxial jet flame is in the same range as found in the nonreacting case, although some potential frequency shifting may be present. Future analysis, which will include proper orthogonal decomposition (POD) and linear stability analysis, will be used to identify dominant (i.e. preferred mode) frequencies and improve our understanding of how flames alter the flow field spectra.

A variety of forced flames were established and studied. Figure 7 shows instantaneous images of both the nonreacting and reacting coaxial jet flame. The forcing frequency was 1.95 kHz, and the forcing amplitude based on the driving voltage was 1.5 V (maximum forcing for the present study was 2.0 V). These results are associated with the injector being located at the pressure node. For the nonreacting case shown in Fig. 7a, the velocity forcing results in a transverse flapping of the liquid core. This has been observed extensively in past nonreacting studies. The pressure node is also associated with an acoustic velocity antinode, which in this case would be a transverse velocity fluctuation in the same direction as the observed jet flapping. The mechanism responsible for this response is not yet clear. Wegener et al. showed that the momentum flux ratio based on transverse velocity fluctuation is not sufficient to explain the jet deflection.³⁰ A strong helical mode may exist, which is difficult to discern when using a line of sight. Further work is required to understand the coupling mechanism for the pressure node regime.

Figure 7b shows the same injector flow and acoustic conditions with a flame present. The flame is seen to be much larger in axial length, in part due to a reduction in fog buildup on the window. Unlike the unforced flame images shown in Fig. 3(b), the liquid core is easier to see and is seen to exhibit transverse wiggles. Intense burning regions at the transverse sides of the flame are seen to evolve and convect downstream. It is very apparent that the presence of acoustic disturbances has had a significant impact on the qualitative features of the flame.

Dynamic mode decomposition was used to extract the spatial structure of flame response at the forcing frequency. The amplitude of the modes may be extracted using the algorithm of Schmid.³¹ The DMD is applied to the image data over the first $10D_1$, to eliminate the lower frequency content in the downstream region. Figure 8 shows the DMD amplitude spectra as a function of frequency for the case with the flame forced at 1.95 kHz, 2.0 V, and a pressure node location. One mode is seen to be dominant over the other modes as is associated with the forcing frequency. Figure 8b shows the real and imaginary components of the spatial mode shape associated with the forcing frequency. The modes clearly represent antisymmetric behavior by the presence of lobes of like sign (red is positive, blue is negative) that are misaligned with respect to the left and right sides of the jet. The real and imaginary components are very similar, although positive (red) and negative (blue) lobes appear to be shifted half a wavelength in the imaginary component relative to the real component. Thus when added together in the reconstruction, a convective process is produced. A similar convective mode may be reconstructed with a pair of POD modes that have certain statistical properties.²³ The relative amplitude of the forced mode compared to the “background” modes is an indicator of strength of the mode in relation to other modes.

Figure 9 shows the DMD decomposition results for the pressure node case at a higher forcing frequency of 3.05 kHz at a forcing amplitude of 2.0 V. The general trend is the same as found for the 1.95 kHz forcing case. The relative amplitude of the forced mode is closer to the background modes, suggesting the forcing response at 3.05 kHz is

somewhat degraded compared to 1.95 kHz. The spatial distribution of the modes is also similar, although as expected, the spatial length scales are smaller for the case forced at a higher frequency.

The forced flames located at the pressure antinode experienced a somewhat degraded response. Figure 10 shows the natural and maximum forcing amplitude cases of a flame located at the pressure antinode. Although very subtle, the images in Fig. 10b exhibit a somewhat organized spiral-like structure in the middle of the images that is not evident in the unforced case. Neither of the cases shown in Fig. 10 exhibit the clear dark jet core as shown for the pressure node forced flame shown in Fig. 7b. The dark core is likely obscured by a more intense flame along the coaxial jet centerline compared to the pressure node forced cases.

The spiral-like nature of the pressure antinode forced flames is further elucidated in the DMD results of Figs. 11 and 12; Figs. 11 and 12 are associated with forcing frequencies of 1.9 and 2.95 kHz, respectively. In both pressure antinode cases, the forced mode amplitude is closer to the background levels relative to the pressure node forcing results. This suggests that the forcing response is somewhat degraded for the pressure antinode case, a trend that is congruent with visual observations of the flame. As found for the pressure node cases, the wavelength of the modes decrease with increasing frequency.

It is interesting to note that the pressure antinode exhibits an apparent helical-like structure. Past results by Teshome²³ and Wegener²⁹ show that the pressure antinode tends to result in symmetrical structures for nonreacting studies. The pressure antinode forcing mechanism as described by Wegener²⁹ and Wegener et al.³⁰ that produces axisymmetric puffing of the outer jet flow would tend to preferentially force an axisymmetric response. Whether these flames have a near field that is axisymmetric or not (that eventually develops into a helical mode) will be explored in future studies.

Unlike the pressure antinode results, the pressure node images show the dark core. This suggests that the flame enhancement for the pressure node does not occur near the injector axis, which would lead to a potential optical interference with respect to viewing the dark core. This suggests that the flapping motion is not axisymmetric but is moving in the plane containing the transverse direction and the axial coordinate.

V. Conclusions

An experimental study was conducted on liquid O₂ / gaseous H₂ coaxial jet flames exposed to transverse standing acoustic waves. The placement of the flame at the pressure node region of the mode shape results in a robust coupling at both frequencies considered. The pressure node excitation results suggest that the flame deflects laterally in the spanwise-axial plane in response to the ambient acoustic velocity perturbations. The response of the flame when placed at the pressure antinode appears to be somewhat reduced compared to the pressure node response. The time-resolved chemiluminescence measurements and dynamic mode decomposition (DMD) of the pressure antinode results indicate a helical-like structure to the flame topology. The forcing mechanism, which is expected to result in axisymmetric pulsing of the annular gas flow, has been found in nonreacting studies to induce axisymmetric structure. The competition/transition between the axisymmetric and helical modes in pressure antinode forced flames will be considered in future work.

References

1. Harrje, D. T., and Reardon, F. H., "Liquid Propellant Rocket Combustion Instability. NASA SP-194," *NASA Special Publication*, Vol. 194, 1972.
2. Chehroudi, B., Talley, D., and Coy, E., "Visual characteristics and initial growth rates of round cryogenic jets at subcritical and supercritical pressures," *Physics of Fluids*, Vol. 14, No. 2, 2002, pp. 850-861.
3. Oswald, M., Smith, J., Branam, R., Hussong, J., Schik, A., Chehroudi, B., and Talley, D., "Injection of fluids into supercritical environments," *Combustion Science and Technology*, Vol. 178, No. 1-3, 2006, pp. 49-100.
4. Leyva, I., Chehroudi, B., and Talley, D., "Dark Core Analysis of Coaxial Injectors at Sub-, Near-, and Supercritical Conditions in a Transverse Acoustic Field," 43rd AIAA/ASME/SAE/ASEE Joint Propulsion Conference & Exhibit, Cincinnati, OH, 8-11 July, 2007.
5. Leyva, I., Rodriguez, J., Chehroudi, B., and Talley, D., "Preliminary Results on Coaxial Jet Sprean Angles and the Effects of Variable Phase Transverse Acoustic Fields," 46th AIAA Aerospace Sciences Meeting and Exhibit, Reno, NV, 7-10 January, 2008.

6. Teshome, S., Leyva, I. A., Talley, D., and Karagozian, A. R., "Cryogenic high-pressure shear-coaxial jets exposed to transverse acoustic forcing," 50th AIAA Aerospace Sciences Meeting Including the New Horizons Forum and Aerospace Exposition, Nashville, TN, 2012.
7. Wegener, J., Leyva, I., Forliti, D., and Talley, D., "Development of a facility for combustion stability experiments at supercritical pressure," 52nd AIAA Aerospace Sciences Meeting, National Harbor, MD, 2014.
8. Davis, D. W., "On the behavior of a shear-coaxial jet, spanning sub-to supercritical pressures, with and without an externally imposed transverse acoustic field," Ph.D., Mechanical Engineering, The Pennsylvania State University, 2006.
9. Rodriguez, J. I., "Acoustic excitation of liquid fuel droplets and coaxial jets," Ph.D., Aerospace Engineering, University of California, Los Angeles, 2009.
10. Yu, Y., Koeglmeier, S., Sisco, J., and Anderson, W., "Combustion instability of gaseous fuels in a continuously variable resonance chamber (CVRC)," 44th AIAA/SAE/ASEE Joint Propulsion Conference & Exhibit, Hartford CT, 21-23 July, 2008.
11. Yu, Y., O'Hara, L., Sisco, J., and Anderson, W., "Experimental study of high-frequency combustion instability in a continuously variable resonance combustor," 47th AIAA Aerospace Sciences Meeting Including The New Horizons Forum and Aerospace Exposition, Orlando, FL, 5-8 January, 2009.
12. Harvazinski, M., Talley, D., and Sankaran, V., "Influence of boundary condition treatment on longitudinal mode combustion instability predictions," 49th AIAA/ASME/SAE/ASEE Joint Propulsion Conference, San Jose, CA, 14-17 July, 2013.
13. Pomeroy, B., Lamont, W., and Anderson, W., "Subscale tool for determining transverse combustion response," 45th AIAA/ASME/SAE/ASEE Joint Propulsion Conference & Exhibit, Denver, CO, 2-5 August, 2009.
14. Wierman, M., Nugent, N., and Anderson, W., "Characterization of an unstable rocket combustor with He addition," 46th AIAA/ASME/SAE/ASEE Joint Propulsion Conference & Exhibit, Nashville, TN, 25-28 July, 2010.
15. Pomeroy, B., Morgan, C., and Anderson, W., "Response of a gas-centered swirl coaxial injector to transverse instabilities," 47th AIAA/ASME/SAE/ASEE Joint Propulsion Conference and Exhibit, San Diego, CA, 31 July-3 Aug, 2011.
16. Rey, C., Ducruix, S., Richecoeur, F., Scoufflaire, P., Vingert, L., and Candel, S., "High frequency combustion instabilities associated with collective interactions in liquid propulsion," 40th AIAA/ASME/SAE/ASEE Joint Propulsion Conference and Exhibit, Fort Lauderdale, FL, 11-14 July, 2004.
17. Richecoeur, F., Scoufflaire, P., Decruix, S., and Candel, S., "Interactions between propellant jets and acoustic modes in liquid rocket engines: experiments and simulations," 42nd AIAA/ASME/SAE/ASEE Joint Propulsion Conference & Exhibit, Sacramento, CA, 9-12 July, 2006.
18. Richecoeur, F., Scoufflaire, P., Ducruix, S., and Candel, S., "High-frequency transverse acoustic coupling in a multiple-injector cryogenic combustor," *Journal of Propulsion and Power*, Vol. 22, No. 4, 2006, pp. 790-799.
19. Richecoeur, F., Ducruix, S., Scoufflaire, P., and Candel, S., "Experimental investigation of high-frequency combustion instabilities in liquid rocket engine," *Acta Astronautica*, Vol. 62, No. 1, 2008, pp. 18-27.
20. Hardi, J., Oswald, M., and Dally, B., "Flame response to acoustic excitation in a rectangular rocket combustor with LOx/H₂ propellants," *CEAS Space Journal*, 2011, pp. 1-9.
21. Hardi, J. S., Oswald, M., and Dally, B., "Acoustic characterisation of a rectangular rocket combustor with liquid oxygen and hydrogen propellants," *Proceedings of the Institution of Mechanical Engineers, Part G: Journal of Aerospace Engineering*, 2012.
22. Hardi, J., Martinez, H., Oswald, M., and Dally, B., "Response of a reacting LOx jet to a transverse acoustic oscillation," *Space Propulsion 2012*, Bordeaux, France, 7-10 May, 2012.
23. Teshome, S., "Droplet Combustion and Non-Reactive Shear-Coaxial Jets with Transverse Acoustic Excitation," Ph.D., Mechanical Engineering, University of California, Los Angeles, 2012.

24. Juniper, M., Sé, and Candel, b., "Edge diffusion flame stabilization behind a step over a liquid reactant," *Journal of Propulsion and Power*, Vol. 19, No. 3, 2003, pp. 332-341.
25. Mayer, W., Schik, A., Sch-aring, M., ffler, and Tamura, H., "Injection and mixing processes in high-pressure liquid oxygen/gaseous hydrogen rocket combustors," *Journal of Propulsion and Power*, Vol. 16, No. 5, 2000, pp. 823-828.
26. Singla, G., Scouflaire, P., Rolon, J-C., and Candel, S., "Flame stabilization in high pressure LO_x/GH₂ and GCH₄ combustion," *Proceedings of the Combustion Institute*, Vol. 31, No. 2, 2007, pp. 2215-2222.
27. Yang, B., Cuoco, F., and Oswald, M., "Atomization and flames in LOX/H2-and LOX/CH4-spray combustion," *Journal of Propulsion and Power*, Vol. 23, No. 4, 2007, pp. 763-771.
28. Herding, G., Snyder, R., Scouflaire, P., Rolon, C., and Candel, S., "Flame stabilization in cryogenic propellant combustion," *Symposium (International) on Combustion*, 1996, pp. 2041-2047.
29. Wegener, J., "Multi-phase combustion and transport processes under the influence of acoustic excitation," Ph.D., Mechanical Engineering, University of California, Los Angeles, 2014.
30. Wegener, J., Forliti, D., Leyva, I., and Talley, D., "Receptivity of a cryogenic coaxial gas-liquid jet to acoustic disturbances," 50th AIAA/ASME/SAE/ASEE Joint Propulsion Conference, Cleveland, OH, 2014.
31. Schmid, P., "Application of the dynamic mode decomposition to experimental data," *Experiments in Fluids*, V. 50, 2011, pp. 1123-1130.

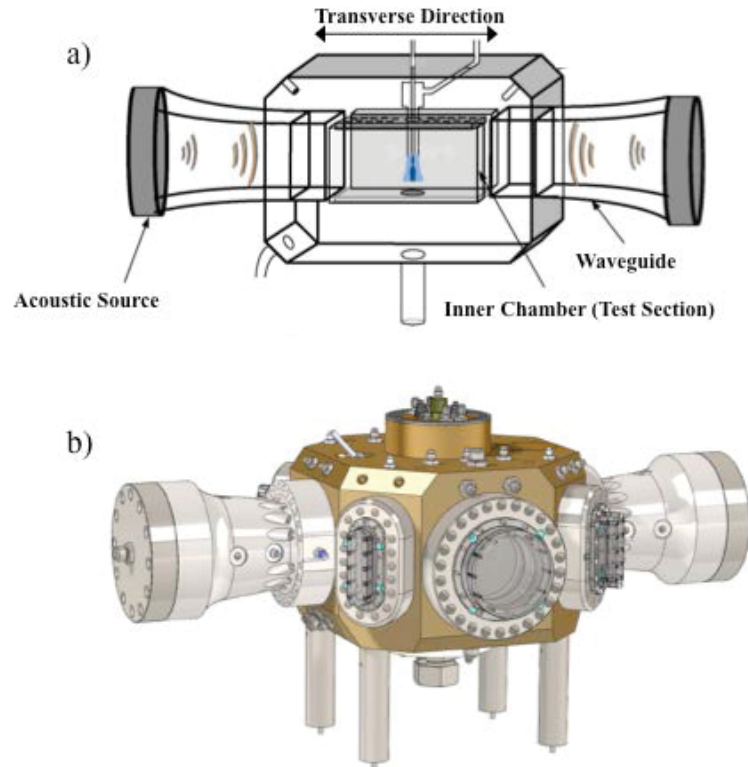


Figure 1. a)Conceptuation and b) schematic of the combustion stability reacting flow facility.

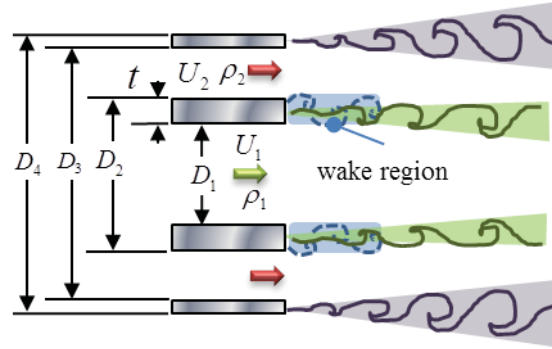


Figure 2. Coaxial jet injector geometry and near field shear flow instabilities.

Table 1: Injector geometry parameters

| Parameter | Value (mm) |
|-----------|------------|
| D_1 | 1.40 |
| D_2 | 2.16 |
| D_3 | 2.82 |
| D_4 | 1.68 |

Table 2: Injector flow conditions

| Parameter | Values |
|--------------------------|-------------------|
| T of inner jet (O_2) | 130 K |
| T of outer jet (H_2) | 250 K |
| J | 2.7 |
| MR | 6 |
| Equivalence ratio | 1.33 |
| Chamber pressure | 3.4 MPa (500 psi) |
| O_2 Re | 4.7×10^4 |
| H_2 Re | 2.2×10^4 |

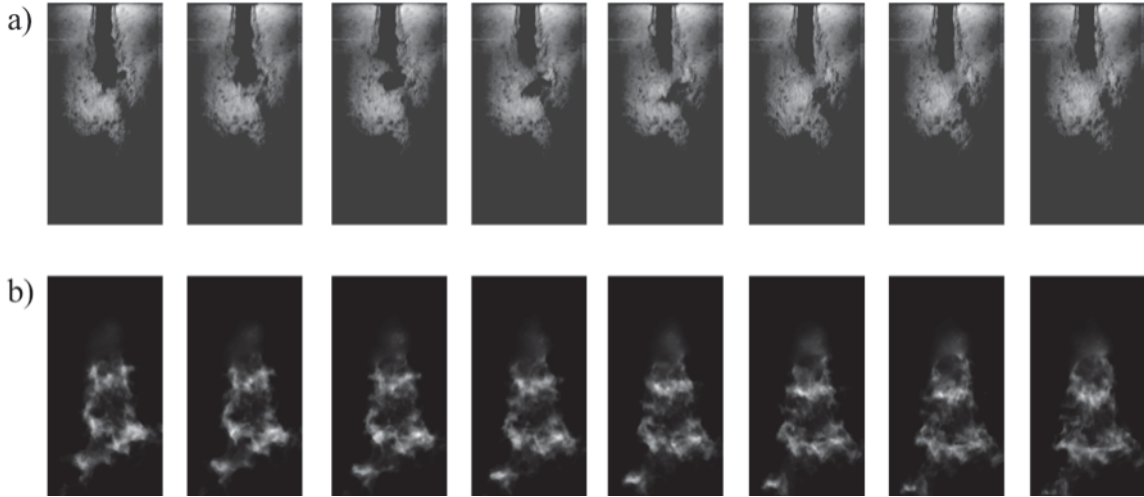


Figure 3. Instantaneous a) backlit and b) unfiltered chemiluminescence images for the unforced condition.

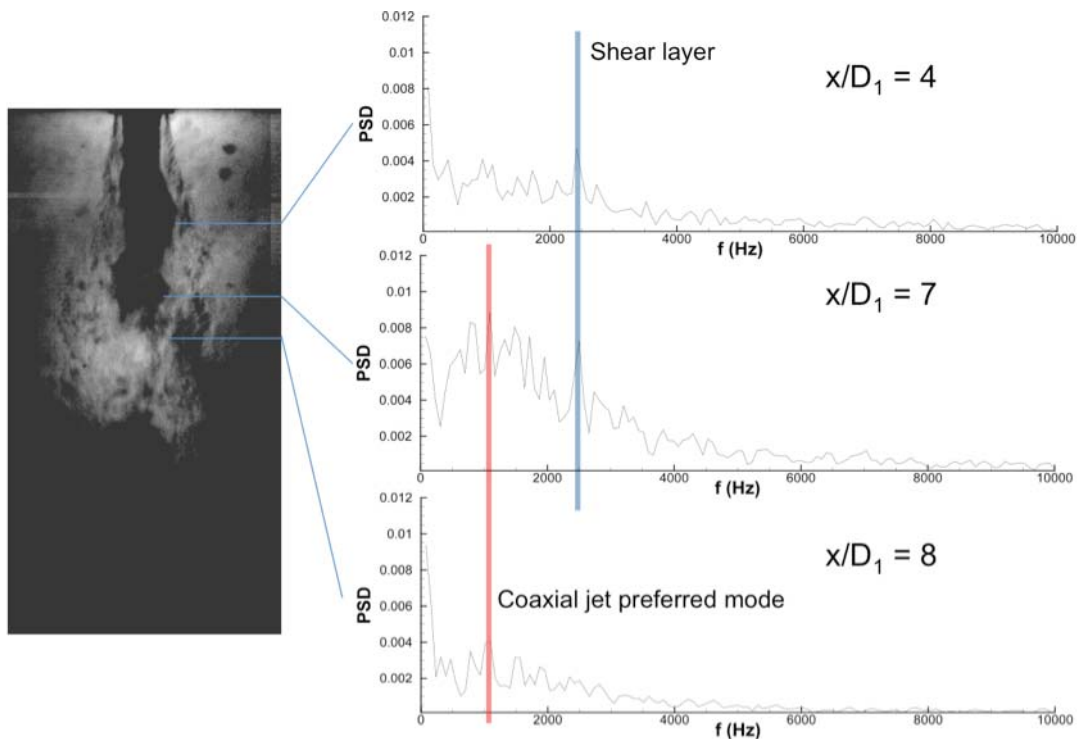


Figure 4. Spectra of the inner shear layer region for the nonreacting unforced flow.

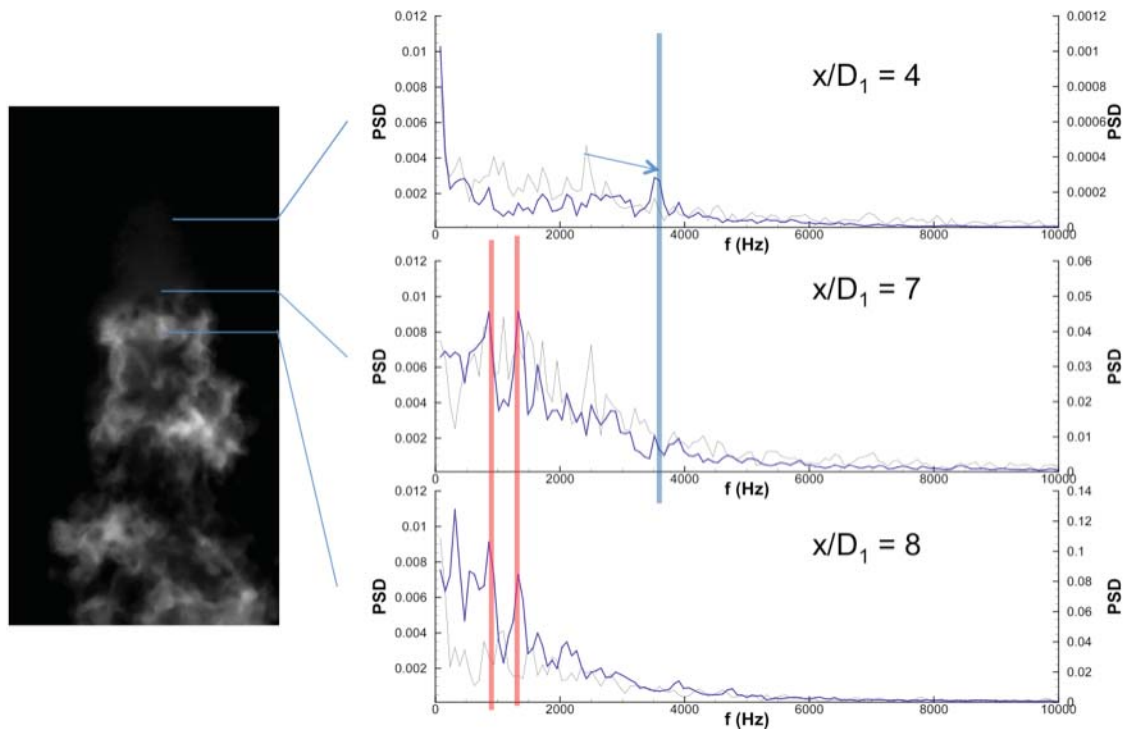


Figure 5. Spectra of the flame region for the reacting unforced flow.

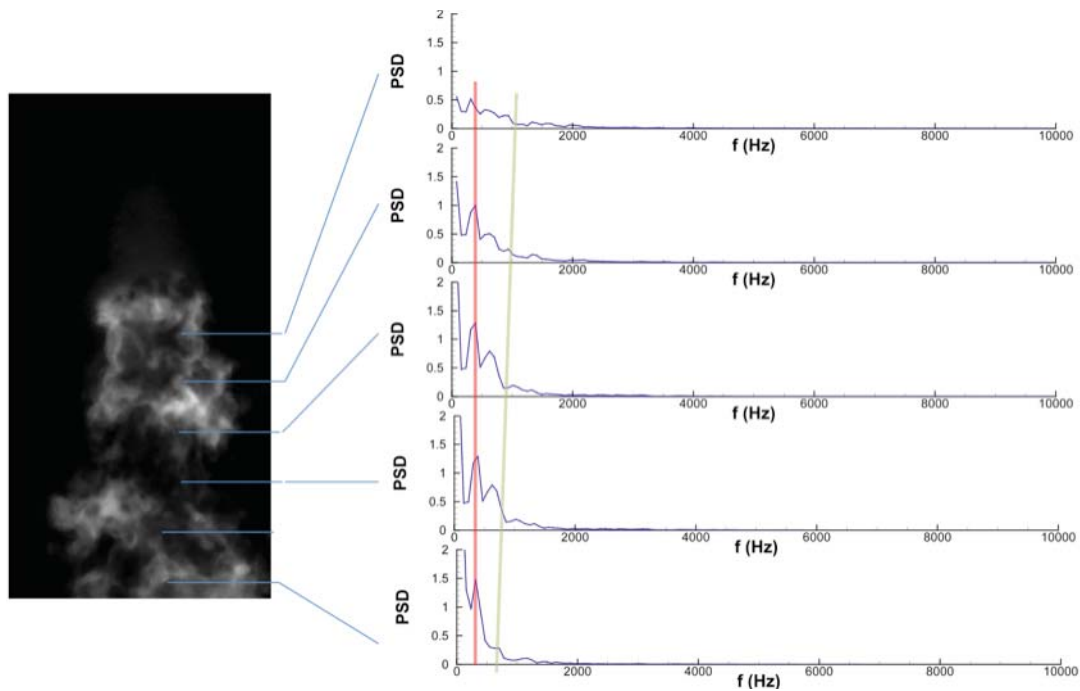


Figure 6. Downstream spectra of the flame region for the reacting unforced flow.

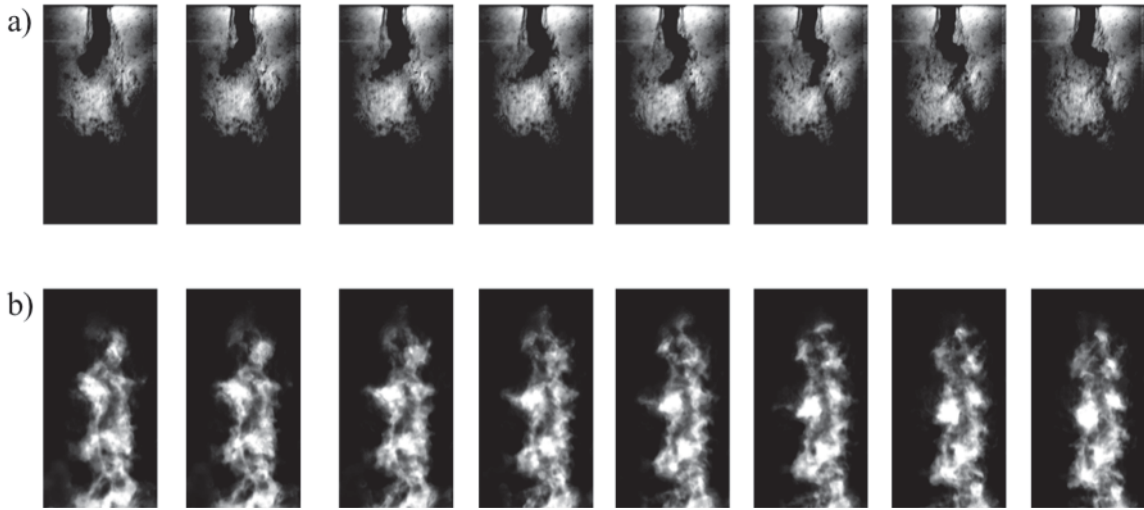


Figure 7. Instantaneous a) backlit and b) unfiltered chemiluminescence images for the pressure node forced condition.

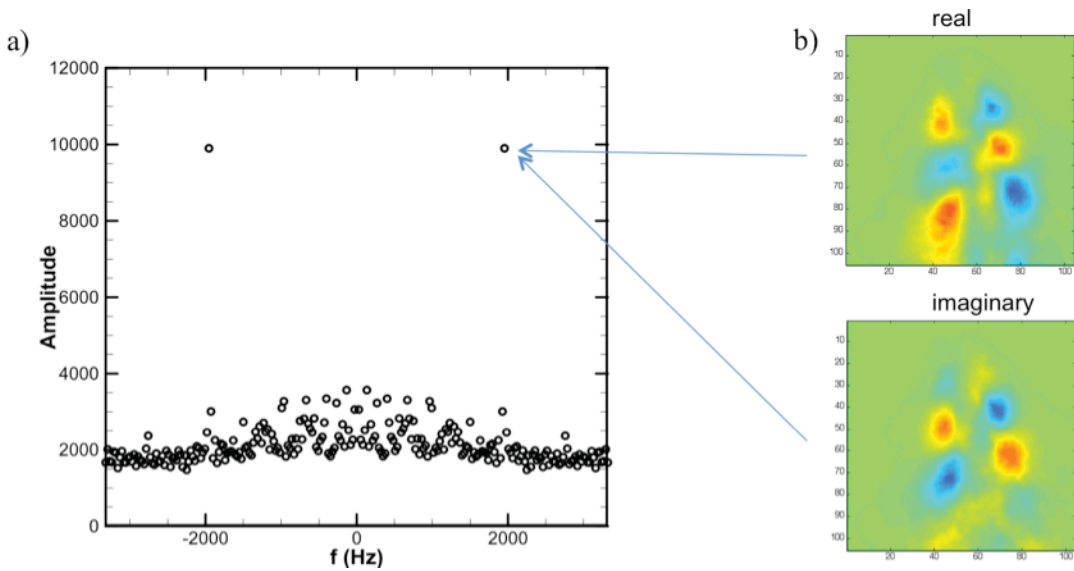


Figure 8. The a) dynamic mode decomposition spectrum and b) forced mode spatial distribution for the maximum pressure node forced flame at 1.95 kHz.

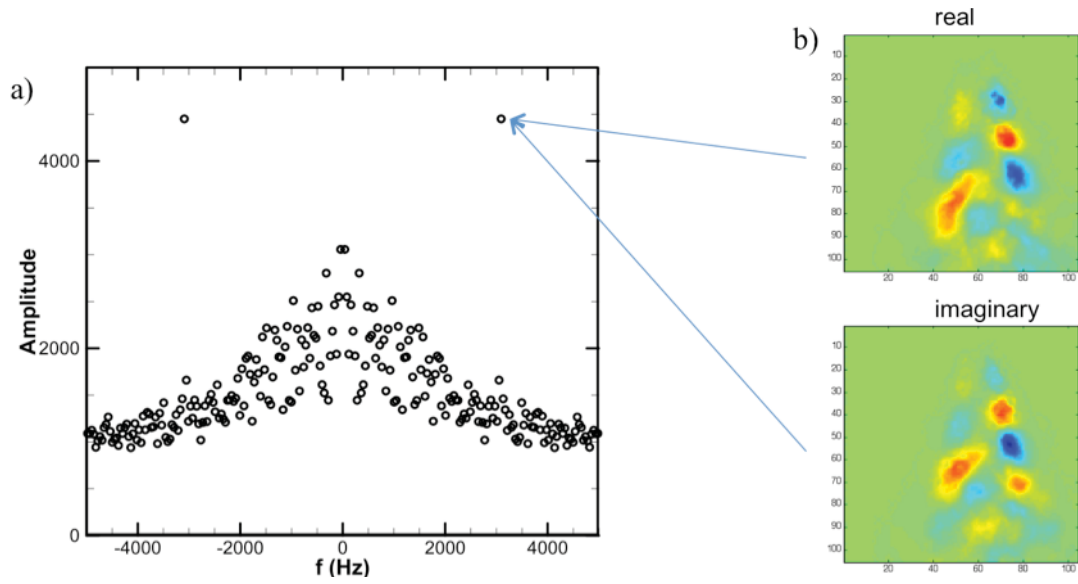


Figure 9. The a) dynamic mode decomposition spectrum and b) forced mode spatial distribution for the maximum pressure node forced flame at 3.05 kHz.

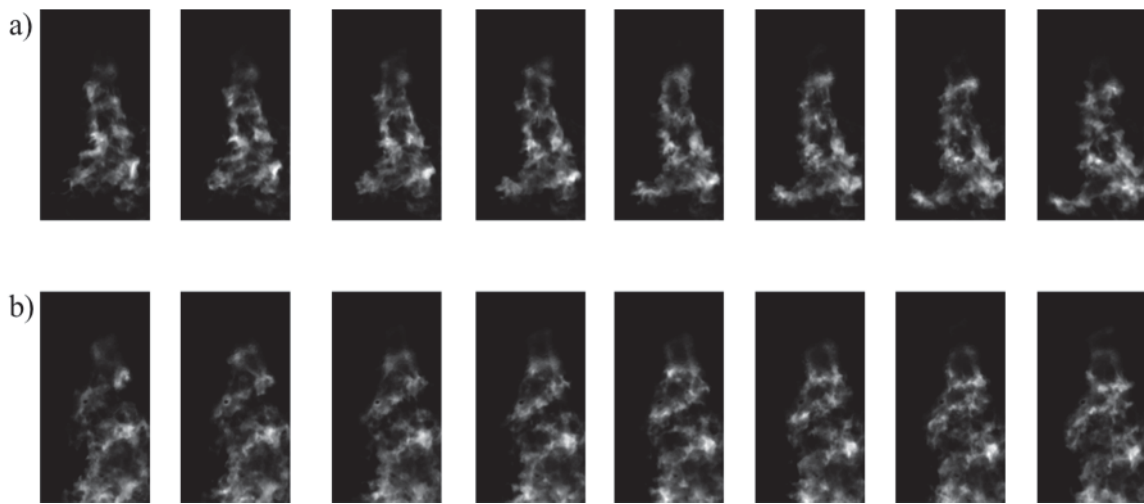


Figure 10. Instantaneous unfiltered chemiluminescence images for the a) unforced and b) pressure anti-node forced condition.

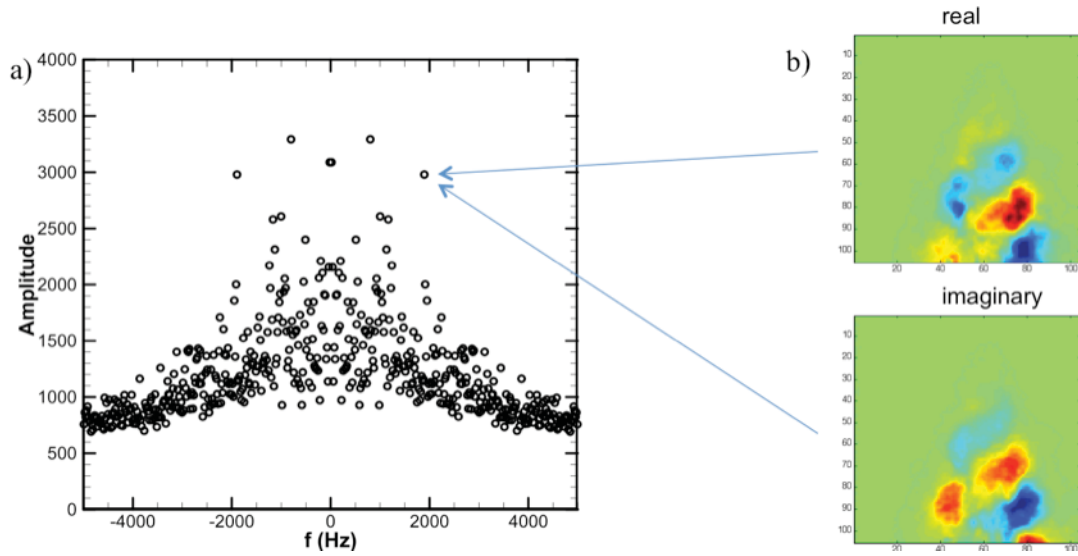


Figure 11. The a) dynamic mode decomposition spectrum and b) forced mode spatial distribution for the maximum pressure antinode forced flame at 1.9 kHz.

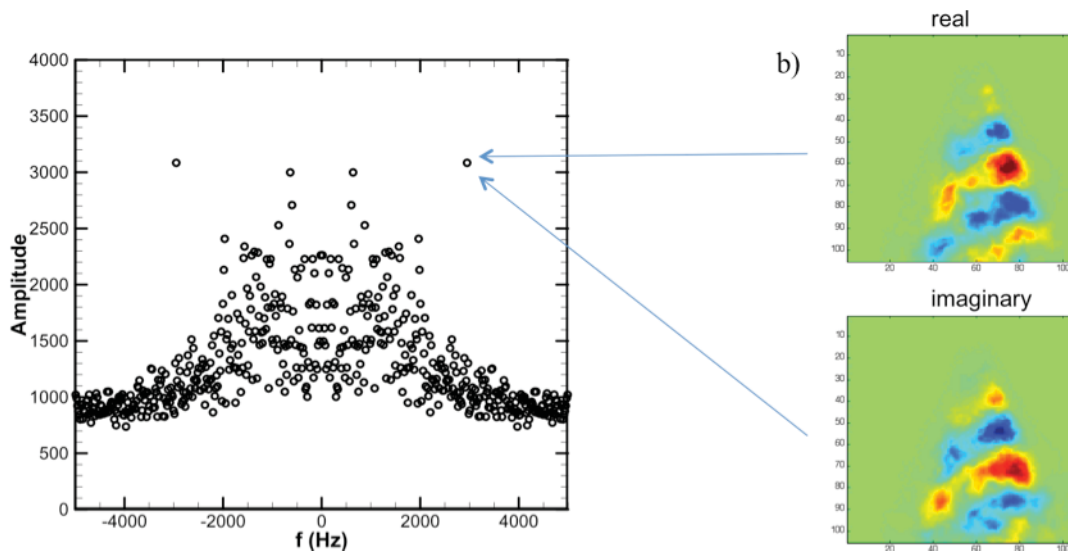


Figure 12. The a) dynamic mode decomposition spectrum and b) forced mode spatial distribution for the maximum pressure antinode forced flame at 2.95 kHz.